Solar Energy 162 (2018) 336–343

Contents lists available at ScienceDirect

Solar Energy

journal homepage: www.elsevier.com/locate/solener

Revealing optoelectronic and transport properties of potential perovskites Cs_2PdX_6 (X = Cl, Br): A probe from density functional theory (DFT)

K.C. Bhamu[a,b], Amit Soni[c], Jagrati Sahariya[d,*]

[a] Physical and Materials Chemistry Division, CSIR-National Chemical Laboratory, Pune 411008, India
[b] Department of Physics, Goa University, Taleigao Plateau, Goa 403206, India
[c] Department of Electrical Engineering, Manipal University Jaipur, Jaipur, Rajasthan 303007, India
[d] Department of Physics, Manipal University Jaipur, Jaipur, Rajasthan 303007, India

ARTICLE INFO

Keywords:
Ab-initio studies
Density functional theory
Optical properties
Transport properties

ABSTRACT

Metal-halide perovskites are rapidly emerging crystalline materials that are reasonably preferred as leading aspirant for applications in optoelectronic and thermoelectric devices. In this paper, we have thoroughly reviewed and performed calculations to reveal optoelectronic and transport properties for a potential newcomer, Cs_2PdX_6 (X = Cl, Br) termed as Cesium Palladium Halides (CPH). Outcome of present computations are compared with available results and a reasonable agreement is recorded. Energy band gap computations performed reveal indirect band gap of 2.29 eV for Cs_2PdCl_6, which substantially reduces to 1.22 eV when 'Cl' is replaced by 'Br'. Optical absorption spectra investigations performed here, in the energy range from 3 to 5 eV confirms effective utilization of these compounds in solar cells and other optoelectronic applications. In addition, the transport properties computations performed using semi-classical Boltzmann theory, shows constant pattern of thermo power near ambient temperature range (200–500 K), which admits possible utilization of these compounds as low temperature thermoelectric materials. Performed ZT calculations demonstrates reasonably good thermoelectric performance for both materials, as there exist minor variation (0.1) in the values over wide temperature ranges i.e. from 100 to 800 K. Further, detailed analysis of transport properties predicts *p*-type semiconducting nature of the present series of materials.

1. Introduction

Drastic increase in global energy demand in past few years, has caused increasing attention of scientific community towards significant utilization of renewable energy sources to bridge this gap. Solar being a leading renewable among all, has played a significant role and hence shown variable performance based on the material used in photovoltaic (PV) modules. Presently, search for appropriate material is key motivation for the researcher's and hence extensive research is carried out in order to identify their potential usage in opto-electronic (Zhang et al., 2015, 2014; Murtaza and Ahmad, 2011; Hao et al., 2014; Sakai et al., 2017; Qiu et al., 2017; Maughan et al., 2016; Ashley et al., 2016; Wang et al., 2015; Xiao et al., 2015; Lee et al., 2014; Brik and Kityk, 2011) and thermoelectric (Hong et al., 2017; Zhao et al., 2014; Liu et al., 2017; Shuai et al., 2017; Sun et al., 2017) applications. Promising utilization of metal halide perovskites (ABX_3 where A = K, Cs, Rb; B = Ge, Pb, Sn; X = Cl, Br, I) for optoelectronic applications (Zhang et al., 2015; Murtaza and Ahmad, 2011; Hao et al., 2014) is also noticed, despite of the fact that they have long term instabilities (Hao et al., 2014; Sakai et al., 2017). In addition, double perovskites with chemical formula, A_2BX_6 of similar family has also been reported as novel candidate for optoelectronic applications (Sakai et al., 2017; Qiu et al., 2017; Maughan et al., 2016; Ashley et al., 2016; Wang et al., 2015; Xiao et al., 2015; Zhang et al., 2014; Lee et al., 2014; Brik and Kityk, 2011). In the past few years, the studies performed are reviewed over here, which envisages their successful optoelectronic utilization. Sakai et al. (2017) have recorded energy band gap of 1.6 eV for Cs_2PdBr_6 using electronic structure calculations and have claimed its excellent prospects in optoelectronic applications and long term stability. Thin film of Cs_2SnI_6 perovskite are grown by Qiu et al. (2017) in view to realize its absorption capability and hence to judge its possible usage in solar cells. Maughan et al. (2016) have elucidated structure property relationships of complex semiconductors $Cs_2Sn_{1-x}Te_xI_6$ and have observed that substitution of Sn by Te accompanies reduction in electrical conductivity, carrier concentration and carrier mobility. Ashley et al. (2016) have described a template to synthesize uniform perovskite nanowires with controlled diameter on transparent conductive substrates. Electronic and optical properties of $Cs_2AX_2Y_4$

* Corresponding author.
E-mail address: jagrati.sahariya@gmail.com (J. Sahariya).

https://doi.org/10.1016/j.solener.2018.01.059
Received 5 October 2017; Received in revised form 16 December 2017; Accepted 17 January 2018

(A = Ge, Sn, Pb; X, Y = Cl, Br, I) have been reported by Wang et al. (2015) to demonstrate their applicability as solar absorbing materials. Xiao et al. (2015) have performed first principle density functional calculations (DFT) to reveal the intrinsic defects of Cs_2SnI_6 perovskite material. Optical properties of Cs_2SnI_6 have been reported by Zhang et al. (2014) to ensure its material integrity. Lee et al. (2014) have deliberated 8% energy conversion efficiency for solar cell material, Cs_2SnI_6 used as absorber layer in practical applications. Lattice constant, ionic radii and electronegativity for a series of cubic structure, A_2XY_6 (A = K, Cs, Rb, Tl; X = tetravalent cation; Y = Cl, Br, I), have been reported by Brik and Kityk (2011) using an empirical model. Above review confirms vibrant research prospects and also global need for appropriate opto-electronic and thermoelectric materials. Present work is motivated on the basis of above literature, which indicates possible utilization of Cesium lead perovskites in large scale industrial applications. On the other hand, environmental hazards reported due to toxic nature of lead element used in these materials has forced researchers to attempt for alternative class of compounds. One of the most appropriate and potential candidate of the same series is Cs_2PdX_6 (X = Cl, Br, I), where lead (Pb) can be replaced by palladium (Pd).

To the best of our knowledge, so far no first principle calculations related to electronic structure, optical and transport properties have been reported yet for $Cs_2Pd(Cl,Br)_6$ perovskite materials. To shed light on this unexplored area, we report a detailed DFT investigations of electronic structure (energy band and density of states (DOS)), optical properties (dielectric tensor, absorption spectra, reflectivity and refractivity) and transport properties (Seebeck coefficient, figure of merit) of these compounds and analyzed their applicability for optoelectronic and thermoelectric applications. Non-toxic behavior of this class of materials will certainly be advantageous for large scale applications, in comparison with existing players Bi_2Te_3 along with its doped derivatives (Poudel et al., 2008; Hu et al., 2016; Zhang et al., 2017; Parker and Singh, 2011a,b; Sharma and Schwingenschlögl, 2016; Saeed et al., 2014; Snyder and Toberer, 2008; Parker and Singh, 2011a,b) and organometallic tri halides $CH_3NH_3PbX_3$ (X = Cl, Br and I) (Chen et al., 2015; Blancon et al., 2017; Protesescu et al., 2015). Both of these materials suffers from large drawbacks: in former case Te is the trace element (Parker and Singh, 2011a,b) and in latter one Pb is the toxic element (Ran et al., 2017) and hence not preferred for large scale applications.

2. Computational details

In this paper, computations are performed for vacancy ordered double perovskites Cs_2PdX_6 (X = Cl, Br) which crystallizes into cubic structure and have space group $Fm\bar{3}m$ (Sakai et al., 2017). In order to attain accurate results, the lattice parameters for the present series were optimized by means of total energy dependent geometry optimization approach (Blaha et al., 2016) and the optimized plots are presented in Fig. 1(a and b). The convergence criterion for total energy, charge and force on the atoms in the unit cell was set to 10^{-5} Ry, 10^{-4} and 1.0 mRy/a.u. Analysis of results plotted reveals lattice parameters for cubic structure Cs_2PdCl_6 (Cs_2PdBr_6) as a = 19.2465 (19.9577) a.u. respectively. The crystalline structure along with its corresponding Brillouin zone (BZ) for both the compounds are presented in Fig. 2(a and b) which briefs exact arrangement used for detailed analysis. To explore overall performance, the computations such as electronic structure, optical properties and transport properties are performed and discussed over here. First phase of computation of structural, electronic and optical properties is carried out using full potential linearized augmented plane (FP-LAPW) method implemented in Wien2k code (Blaha et al., 2016). All computations were performed using PBE-sol (Perdew et al., 2008) followed by one of the most accurate Tran and Blaha's (2009) modified Becke-Johnson (TB-mBJ) potential for self-consistency. The plane wave cut-off value $R_{MT} \times K_{MAX} = 7$, maximum radial expansion $l_{max} = 10$ and 2000 k-points (12 × 12 × 12 mesh size) are the values

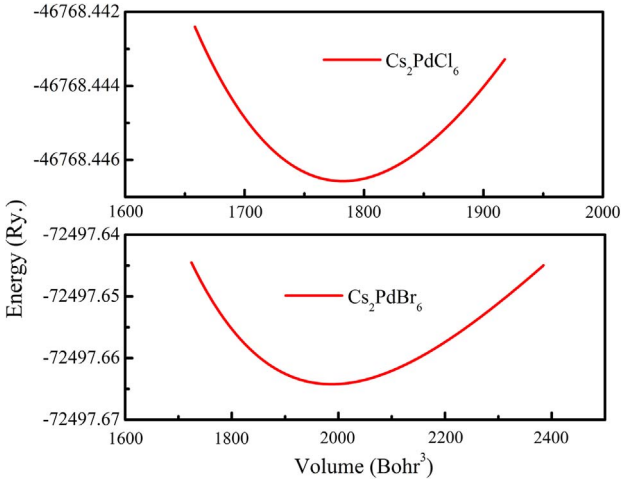

Fig. 1. Energy v/s volume optimization curve for Cs_2PdCl_6 and Cs_2PdBr_6.

used for performing present self-consist calculations. Second phase of these calculations, are performed in view to elucidate transport properties for the present series. The code used for these computations is BoltzTraP code which is based on constant scattering time approximation (CSTA) and rigid band approximation (RBA) (Madsen and Singh, 2006; Reshak et al., 2014; Reshak and Auluck, 2015). In interest to obtain more accurate results for transport properties, we have used over here ~~a~~ very high k-mesh (40,000) sampling in Irreducible Brillouin-zone (IBZ).

3. Results and discussion

3.1. Energy bands & density of states

In view to analyze possible utilization area of these compounds, we have to first visualize their key physical features by means of studies performed such as energy band structure and DOS. Energy band structure computations for Cs_2PdX_6 (X = Cl, Br) are performed over here along with high symmetry directions of first Brillouin Zone (BZ) using mBJ potential and are presented along with total DOS in Fig. 3(a and c). Results obtained indicate that for both compounds, valance band maximum (VBM) and conduction band minimum (CBM) falls at Γ and X points, respectively which clearly proves indirect band gap nature of these perovskite compounds. Results presented here indicates that, conduction band minimum will be shifted towards lower energy range when 'Cl' is replaced by 'Br' in present combination and hence reveals considerable band gap reduction. This reduction in band gap magnitude is due to quantum size effect reported earlier (Deotale and Nandedkar, 2016). Energy band gap resulted from present mBJ calculations shows varied output from 2.29 eV (Cs_2PdCl_6) to 1.21 eV (Cs_2PdBr_6). In addition, band gap computed using present approaches along with available results (Sakai et al., 2017) are collated in Table 1. Among both compounds, reporting related to band gap is existing only for Cs_2PdBr_6 (Sakai et al., 2017), which is observed to have close agreement with present computations. Although, there exist difference in band gap values of present computations when compared with available experimental calculation (Sakai et al., 2017), but this mainly occurs due to well-known self-interaction error of DFT (Ciofini et al., 2005; Singh, 2010). To the best of our knowledge, no band gap results are quoted for Cs_2PdCl_6 compound previously, and hence present calculations becomes significantly important for future reference. Results obtained shows similar band splitting patterns for both the compounds and except the energy values, no major change is recorded. Energy band shifting to reduced energy levels is observed in conduction region, when 'Cl' is replaced by 'Br' and the same is reflected with significant variation in band gap as shown in Table 1. It is worth mentioning that,

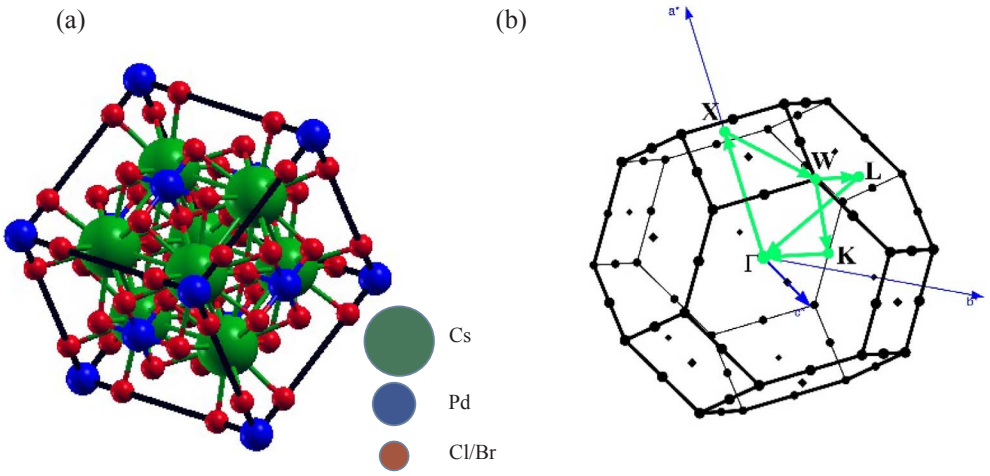

Fig. 2. (a) Crystal structure and (b) Brillouin zone along with high symmetry directions for $Cs_2Pd(Cl,Br)_6$.

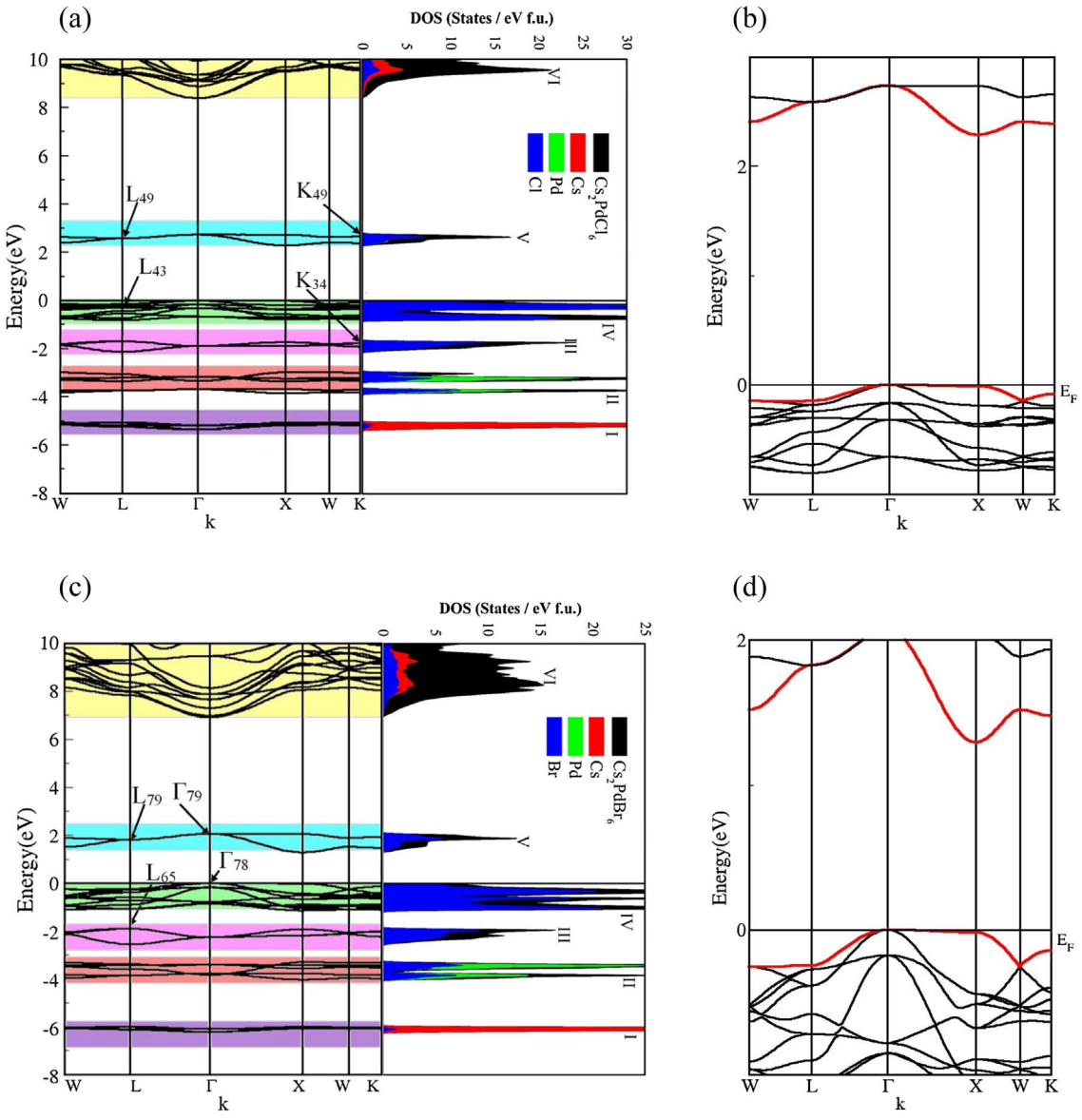

Fig. 3. Energy band structure and TDOS, for (a) Cs_2PdCl_6 and (c) Cs_2PdBr_6 using FP-LAPW-mBJ scheme. Energy bands in small energy range are shown in (b) Cs_2PdCl_6 and (d) Cs_2PdBr_6 for more clear presentation of VBM and CBM. Computations are performed along high symmetry directions of First Brillion Zone.

Table 1
Energy band gap (E_g eV) for Cs_2PdCl_6 and Cs_2PdBr_6 along with previous available calculations.

Approach ↓	Cs_2PdCl_6		Cs_2PdBr_6	
	Present work	Reported data	Present work	Reported data
mBJ	2.29 eV	–	1.22 eV	1.6 eV[a]
PBEsol	1.36 eV	–	0.50 eV	–

[a] Sakai et al. (2017).

here substantial difference in band gap magnitude is recorded for mBJ and PBEsol calculations. Difference resulted is well-known (Tran and Blaha, 2009; Kumar et al., 2017) and occurs due to self-interaction error observed in PBEsol, which causes band gap underestimation. mBJ calculation is more accurate, orbital independent, uses overall system by adopting hybrid functional nature and works on total energy optimization (Tran and Blaha, 2009; Kumar et al., 2017), hence certainly provides improved band gap. Existence of energy bands for both the compounds is elaborated with the help of atom specific total density of states (TDOS) for Cs_2PdX_6(X = Cl, Br) and for this energy bands are divided into different regions from I to VI in Fig. 3(a and c). Detailed analysis of band existence requires correlation between energy bands, TDOS and partial DOS plotted in Figs. 3(a and c) and 4(a and b). The lowermost bunch (Region I) of energy bands available for both compounds are originated mainly due to Cs atom and here the major contribution of Cs-p states is recorded. Region II reports major hybridization of p and s-states of Cl /Br atoms, in addition to this minor involvement of s/d states of Pd atom is also observed. Region III shows significant mixing of p-states of Cl/Br and Pd atoms, here minor involvement of s-states of Cl/Br and d-states of Pd is also recorded. Energy bands available just below Fermi (E_F) level (Region IV) comprises of major hybridization between p-states of Cl/Br and p/d-states of Pd. Bands available just above Fermi level (Region V) resulted due to d-states of Pd along with p-states of Cl/Br. The uppermost group of energy bands (Region VI) are reported to have major mixing of d, s/p/d and s-states of Cs, Cl/Br and Pd atoms respectively. In addition, minor availability of s/p and p/d-states of Cs and Pd is observed. In all availability of energy bands for both the compounds are observed to have similar nature and contribution pattern of the atom states.

3.2. Optical properties

In interest to ascertain utilization of these compounds in opto-electronic applications we have performed detailed investigations of their optical behavior. Broadly, dielectric function calculations plays a significant role among all and can be correlated with electronic structure for required justifications. The expression for dielectric function '$\varepsilon(\omega)$' will be given as:

$$\varepsilon(\omega) = \varepsilon_1(\omega) + i\,\varepsilon_2(\omega), \quad (1)$$

here, $\varepsilon_1(\omega)$ and $\varepsilon_2(\omega)$ are representing the real and imaginary

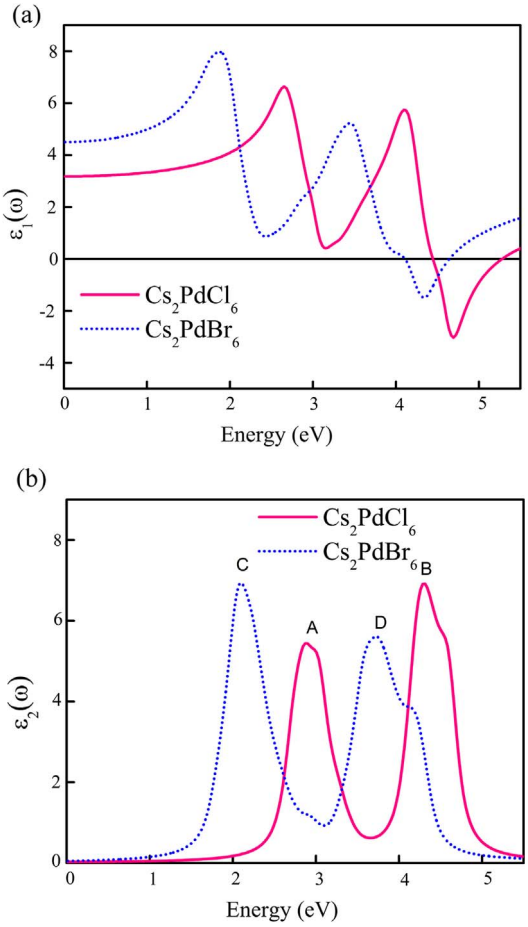

Fig. 5. Parallel and perpendicular components of (a) Real $\varepsilon_1(\omega)$ and (b) imaginary $\varepsilon_2(\omega)$ components of dielectric tensor of Cs_2PdCl_6 and Cs_2PdBr_6 respectively.

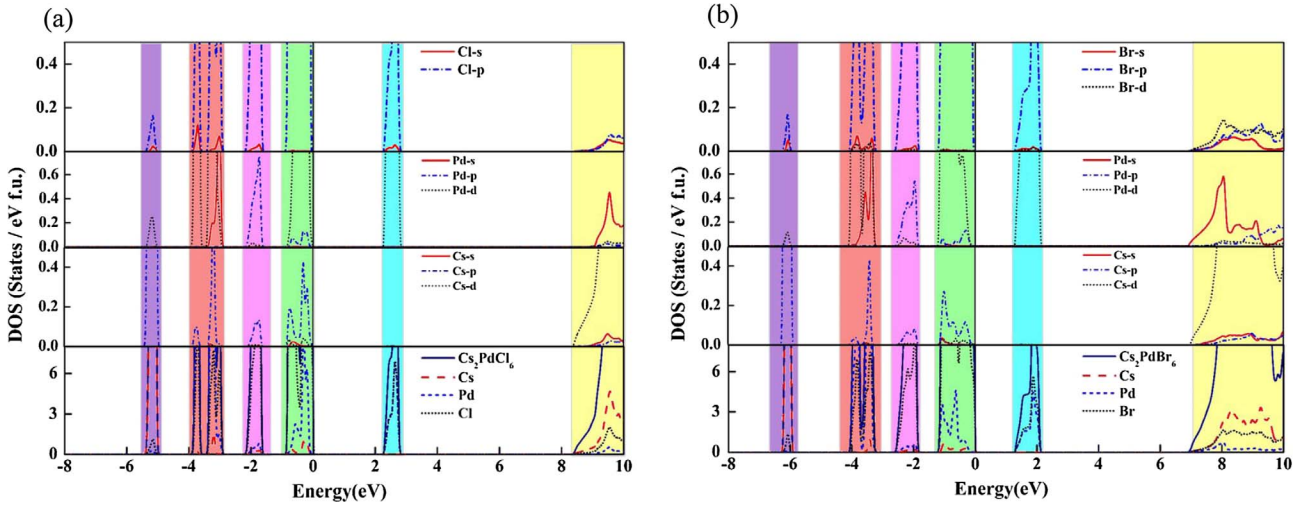

Fig. 4. Total and Partial DOS plotted for (a) Cs_2PdCl_6 and (b) Cs_2PdBr_6 using FP-LAPW-mBJ scheme indicating major possible contributions.

Table 2
The possible dominant transitions corresponding to peaks in $\varepsilon_2(\omega)$ spectra. The numbering of bands is based on the convention of theWien2k software.

Cs_2PdCl_6			Cs_2PdBr_6		
Peak	Peak position (eV)	Dominant transition	Peak	Peak position (eV)	Dominant transition
A	2.89	$L_{43} \rightarrow L_{49,50}$	C	2.08	$\Gamma_{78} \rightarrow \Gamma_{79}$
B	4.31	$K_{34} \rightarrow K_{49}$	D	3.71	$L_{65,66} \rightarrow L_{79}$

components of dielectric tensor, respectively. It is worth mentioning that, as both the compounds studied bears cubic structure, hence will possess only one non-zero component of second order dielectric tensor. Real $[\varepsilon_1(\omega)]$ and imaginary $[\varepsilon_2(\omega)]$ components plotted for Cs_2PdX_6(X = Cl, Br) are represented in Fig. 5(a and b), and the analysis of threshold energy for Cs_2PdCl_6 is 2.05 eV which reduces to 1.07 eV for Cs_2PdBr_6. These points correspond to the transitions of electron from valence band maximum to conduction band minimum i.e. Γ → X points of BZ. Energy peaks observed in $\varepsilon_2(\omega)$ curves [Fig. 5(b)] are originated due to inter-band transitions taking place as indicated in individual band structures [Fig. 3(a and b)]. Peaks recorded for Cs_2PdCl_6 are A (2.89 eV) and B (4.31 eV) and the corresponding responsible electron transitions are $L_{43} \rightarrow L_{49,50}$ and $K_{34} \rightarrow K_{49}$ respectively. Former (2.89 eV) may be originated due to electron transition from d-states of Pd to p-states of Cl and the latter (4.31 eV) occurs due to p-states of Pd and Cl. For Cs_2PdBr_6, peaks recorded are C (2.08 eV) and D (3.71 eV) and the corresponding possible transitions are Cs (p) → Br (p) and Pd (p) → Br (p) respectively. Transitions recorded and corresponding peaks for both the compounds are collated in Table 2 which clearly explains the dominant transitions. Real part $[\varepsilon_1(\omega)]$ of dielectric tensor, can be obtained by using Kramers-Kronig relations (Blaha et al., 2016) given by:

$$\varepsilon_1(\omega) = 1 + \frac{2}{\pi} P \int_0^{\infty} \frac{\omega' \varepsilon_2(\omega')}{\omega'^2 - \omega^2} d\omega'. \quad (2)$$

here, P represent the principal integral. Static dielectric constant $\varepsilon_1(0)$ recorded (Table 3) for Cs_2PdCl_6 is 3.18, which is observed to be raised till 4.50, when 'Br' is substituted in place of 'Cl' [Fig. 5(a)]. Computations performed for $\varepsilon_1(0)$ are in accordance with the Penn model (1962), which shows inverse relationship with energy gap. To deduce detailed optical behavior, responsible properties such as: absorption coefficient $[\alpha(\omega)]$, reflectivity $[R(\omega)]$ and refraction $[\eta(\omega)]$ spectra for Cs_2PdX_6 (X = Cl, Br) are computed using following relations:

$$R(\omega) = \frac{[n-1]^2 + k^2}{[n+1]^2 + k^2} \quad (3)$$

$$n(\omega) = \sqrt{\{\varepsilon_1^2(\omega) + \varepsilon_2^2(\omega) + \varepsilon_1(\omega)\}/2} \quad (4)$$

$$\alpha(\omega) = \sqrt{2}\omega[\sqrt{\varepsilon_1^2(\omega) + \varepsilon_2^2(\omega)} - \varepsilon_1(\omega)]^{1/2} \quad (5)$$

Results obtained are presented over here in Figs. 6–8. Absorption edges (Fig. 6) are observed at 2.02 (Cs_2PdCl_6) and 1.21 eV (Cs_2PdBr_6), which are close with respective energy gaps. In view to explore effective utilization in photonic/opto-electronic applications, the integrated absorption coefficient (IAC) for these compounds is computed in most intense region (3–5 eV) of solar radiations (visible region). Results obtained are 85.676 (Cs_2PdCl_6) and 69.458 (Cs_2PdBr_6), which proves Cl based halides as most promising material for opto-electronic applications. Reflection and refraction spectra shows similar pattern for both the compounds in the energy range from 0 to 5 eV. Total reflection reported increases from 8% (Cs_2PdCl_6) to 13% (Cs_2PdBr_6) at 0 eV (Fig. 7) as represented in Table 3. Similarly, the increase in refractive index for present series is observed from 1.78 (Cl) → 2.12 (Br). Above

Table 3
Calculated dielectric constant $\varepsilon_1(0)$, reflectivity R(0) and refractive index n(0) for Cs_2PdCl_6 and Cs_2PdBr_6 using mBJ scheme.

Compound	$\varepsilon_1(0)$	R(0)	η(0)
Cs_2PdCl_6	3.18	7.92%	1.78
Cs_2PdBr_6	4.50	12.90%	2.12

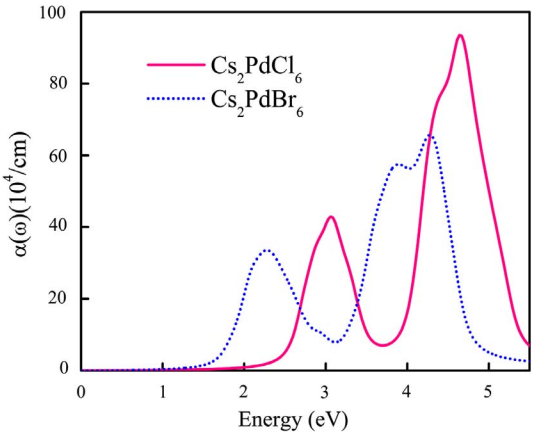

Fig. 6. Absorption coefficient '$\alpha(\omega)$' for $Cs_2Pd(Cl,Br)_6$ computed using mBJ potential.

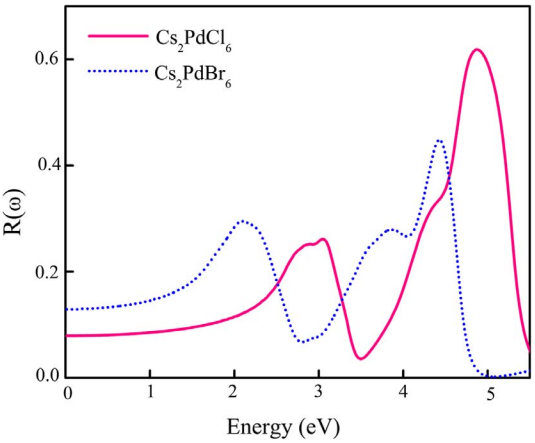

Fig. 7. Energy dependent reflectivity spectra '$R(\omega)$' for $Cs_2Pd(Cl,Br)_6$ computed using mBJ potential.

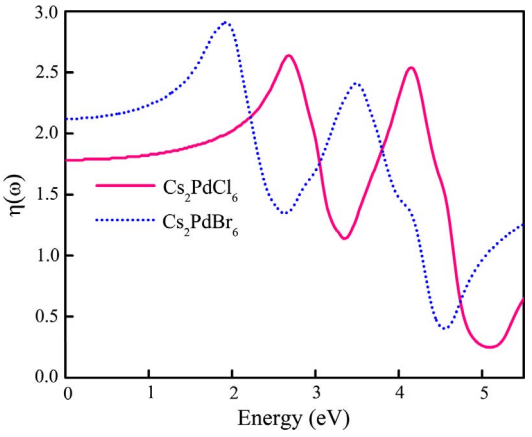

Fig. 8. Real part of refractive index '$\eta(\omega)$' for $Cs_2Pd(Cl,Br)_6$ computed using mBJ potential.

discussed static constants $\varepsilon_1(0)$, $R(0)$ and $\eta(0)$ are mentioned in Table 3, this will also validate their relationship i.e. $\eta(0) = \sqrt{\varepsilon_1(0)}$.

3.3. Transport properties

Transport properties of present compounds is investigated which reveals the conversion efficiency for any thermoelectric material. The same can be characterized by using dimensionless quantity, figure of merit (ZT) under CSTA and RBA approximations. Mathematical expressions for ZT will be given by the relation:

$$ZT = S^2\sigma T/k, \tag{6}$$

here, symbols S, σ and T represents Seebeck coefficient or thermopower, electrical conductivity and absolute temperature, respectively. Symbol 'k' represents thermal conductivity of the material and is composed of electronic (k_{el}) and lattice (k_{ph}) contributions. To achieve higher magnitudes of ZT, the desired values of S, σ and T should be higher and thermal conductivity 'k' should be lower. As per standard BoltzTraP code, 'k_{ph}' is ignored and only electronic part of the thermal conductivity is taken into account. Temperature and chemical potential dependent canonical expressions of S, and σ are given by (Madsen and Singh, 2006; Reshak et al., 2014; Reshak and Auluck, 2015)

$$S_{\alpha\beta}(T,\mu) = \frac{1}{eT\Omega\sigma_{\alpha\beta}(T,\mu)} \int \sigma_{\alpha\beta}(\varepsilon)(\varepsilon-\mu)\left[-\frac{\partial f_\mu(T,\varepsilon)}{\partial\varepsilon}\right]d\varepsilon, \tag{7}$$

and,

$$\sigma_{\alpha\beta}(T,\mu) = \frac{1}{\Omega} \int \sigma_{\alpha\beta}(\varepsilon)\left[-\frac{\partial f_\mu(T,\varepsilon)}{\partial\varepsilon}\right]d\varepsilon, \tag{8}$$

here, Ω, f_μ, μ and $\sigma_{\alpha\beta}(\varepsilon)$ are the, volume of the unit cell, fermi-distribution function, chemical potential and the energy projected transport distribution tensor respectively. The variables used 'α' and 'β' represents the tensor indices. The energy projected transport distribution tensor can further be written as

$$\sigma_{\alpha\beta}(\varepsilon) = \frac{e^2}{N}\sum_{i,k} \tau_{i,k}\upsilon_\alpha(i,k)\upsilon_\beta(i,k)\frac{\partial(\varepsilon-\varepsilon_{i,k})}{d\varepsilon}, \tag{9}$$

where N, τ, e represents the number of k points sampling, relaxation time and electron charge, respectively, $\upsilon_\alpha(i,k)$ and $\upsilon_\beta(i,k)$ are group velocities and $\varepsilon_{i,k}$ is electron-band energies with band index i and k wave vector. Seebeck coefficient is playing significant role, hence preferred to describe thermoelectric performance of these materials. Seebeck coefficient or thermopower is described as the ratio of voltage difference to that of temperature difference which is computed presently under linear response regime (Geisler et al., 2017). Modifications over a complete temperature range (100–800 K) in magnitude of 'S' is recorded and presented (Fig. 9(a)) over here for both compounds. Detailed analysis reveals similar pattern for both compounds below room temperature while above that, higher magnitudes are resulted for Cs_2PdBr_6. This difference in Seebeck coefficient or thermopower can be understood in terms of band gap which is governed with temperature variation and carrier concentration. Thermopower is highly sensitive to the shape of density of states near band edge (Rhyee et al., 2010; Parker and Singh, 2011a,b) and increase in temperature will directly affects the DOS. Other significant observation is the gradual reduction in power factor with increase in temperature which can be understood by cancellation of induced Seebeck voltage due to movement of both type of charge carriers (Snyder and Toberer, 2008). Absolute values of Seebeck coefficient at room temperature recorded for $Cs_2Pd(Cl,Br)_6$ are 205.497 (232.877) μV/K respectively. Depending upon the nature of charge carriers the magnitude of Seebeck coefficient may be positive or negative [Reshak and Auluck, 2015; Rhyee et al., 2010]. From Fig. 9(a), Seebeck coefficient is observed to be positive for entire temperature range of both compounds and hence indicates them as p-type semiconductor. In addition, for more clear understanding regarding conductivity nature, hole and electron effective mass computations are also performed and presented in Table 4. Results indicates that, effective mass of valence band is higher than that of conduction band, which supports the p-type conductivity nature for both compounds. Small variation (~50 μV/K) in its value over a temperature range of 200–300 K indicates good thermo-electric performance and possible effective utilization in cooling applications (Parker and Singh, 2011a,b).

Figure of merit (ZT), computations are presented in Fig. 9(b), for both compounds in the temperature range 100 K to 800 K. Analysis of this reveals highest ZT values for Cs_2PdCl_6 (Cs_2PdBr_6) as 0.80 (0.84) and 0.71 (0.76) at 100 K and 800 K, respectively. Other variations are: 0.78 at 300 K, at temperature below ~200 K both compounds trace the trend of Seebeck coefficient, in range 305 K–555 K, values of Cs_2PbCl_6 become higher while gradual reduction in magnitudes is recorded for Cs_2PdBr_6 and in interval 200 K to 370 K, almost constant nature is observed for Cs_2PdCl_6. Among both compounds, irregular behavior of ZT is resulted for Cs_2PdCl_6 and one possible reason for this trend may be its higher indirect band gap range. ZT plotted with temperature in Fig. 9(b), reflects constant magnitude for the temperature range (200 K-400 K) for Cs_2PbCl_6, but in Cs_2PdBr_6 gradual decreasing nature is recorded. Dominant reason for this nature difference is direct relationship of temperature with band gap and electrical conductivity of the materials as shown below:

$$E_g(T) = E_g(0) - \frac{\alpha T^2}{T+\beta} \tag{10}$$

As indicated above, temperature increase causes reduction in band gap of the material and hence magnitude of ZT. Band gap range of Cs_2PdBr_6 (1.22 eV) is lower than that of Cs_2PdCl_6 (2.29 eV) which also affects their thermoelectric performance. Cs_2PdCl_6 is having higher band gap hence with temperature increase shows nearly constant behavior of ZT in 200–400 K range, as temperature increase beyond 400 K electron-hole bipolar diffusion effect starts dominating, which causes sudden variation, later on general reduction is observed in magnitude of ZT. In general, the larger values of ZT at lower temperature side indicates lower thermal conductivity and higher electrical conductivity (Fig. 9(c) and (d)) for these compounds. Trends recorded for ZT predicts efficient conversion of heat into electricity for the given material and largely depends on exact approximation of S,ρand κ values. This indicates, further improvement possibilities in the calculated values of ZT with the help of more accurate model in comparison with the present system.

4. Conclusion

In the present paper, we have demonstrated analysis of electronic, optical and transport properties of potential photosensitive perovskites Cs_2PdX_6 (X = Cl, Br) for the first time. For more accuracy of present density functional investigations, the calculations are performed using one of the most accurate mBJ exchange correlation potential implemented under full potential linearized augmented plane wave method. Results obtained are observed to have reasonable agreement with available experimental calculations and reveals indirect band gap 2.29 eV (Cs_2PdCl_6) and 1.21 eV (Cs_2PdBr_6) for both the compounds. Analysis of absorption spectra in visible energy range (3–5 eV) along with other optical responses affirms good optical and thermoelectric performance of cesium palladium halides for practical applications at ambient temperature. Further improvements in computed thermoelectric response may be resulted by adopting systematic techniques such as carrier concentration tuning and reducing lattice thermal conductivity. More experimental work in this area related to device fabrication for optoelectronic and cooling thermal devices will certainly be helpful in fulfilling government and industrial goals.

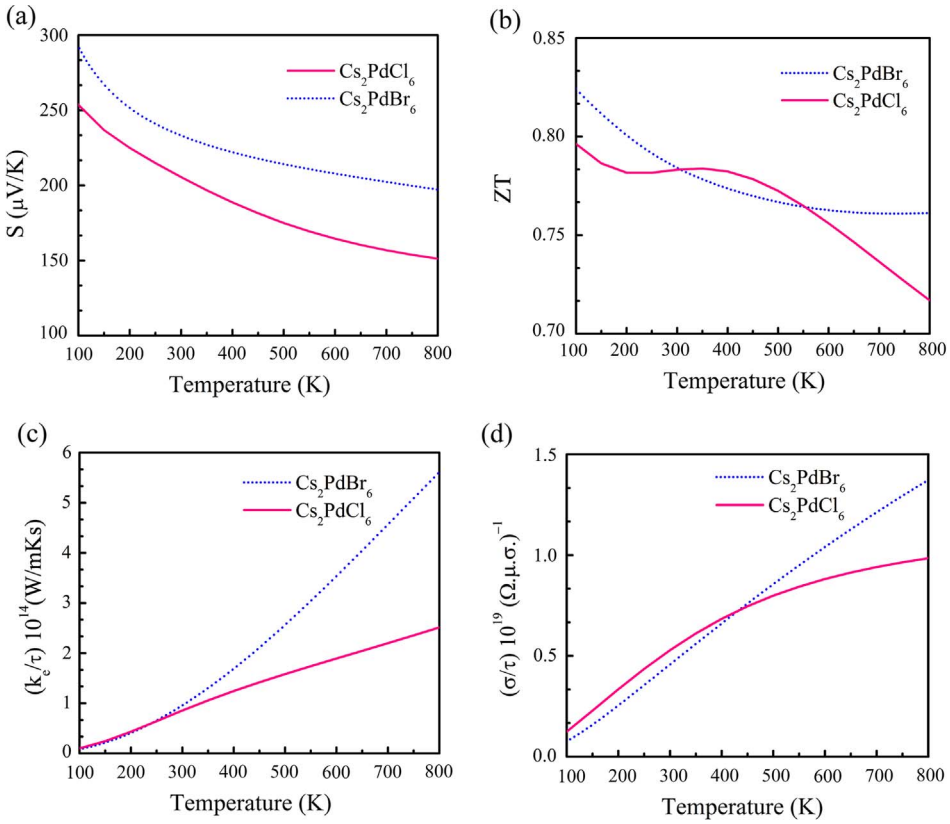

Fig. 9. Variation of (a) Seebeck coefficient, (b) figure of merit, (c) thermal conductivity and (d) electrical conductivity with temperature for $Cs_2Pd(Cl,Br)_6$.

Table 4
Calculation of effective mass (m^*) under parabolic band approximation. Here lh, hh and CBM in the subscript represents the light hole, heavy hole and conduction band minimum, respectively.

	m^*_{hh}	m^*_{lh}	m^*_{CBM}
Cs_2PdCl_6	4.76	2.20	1.27
Cs_2PdBr_6	3.07	1.20	0.60

Acknowledgement

We are grateful to Prof. P. Blaha for providing the Wien2k code. Present work is financially supported by SERB, New Delhi, India under National PDF scheme (Letter No: PDF/2017/002876) and through financial support provided by Manipal University Jaipur under seed grant project (Letter No: EF/2016/05-04). KCB also acknowledge UGC, New Delhi (India) for Dr. D. S. Kothari Postdoctoral Fellowship [No.4-2/2006(BSR)/PH/13-14/0113] and resources of National Energy Research Scientific Computing Center (NERSC), under Contract No. DE-AC02-05CH11231.

References

Ashley, M.J., O'Brien, M.N., Hedderick, K.R., Mason, J.A., Ross, M.B., Mirkin, C.A., 2016. Templated synthesis of uniform perovskite nanowire arrays. J. Am. Chem. Soc. 138, 10096–10099.

Blaha, P., Schwarz, K., Madsen, G.K.H., Kvasnicka, D., Luitz, J., 2016. Wien2K Code, An Augmented Plane Wave Plus Local Orbitals Program for Calculating Crystal Properties. Vienna University of Technology, Vienna, Austria.

Blancon, J.C., Tsai, H., Nie, W., Stoumpos, C.C., Pedesseau, L., Katan, C., Kepenekian, M., Soe, C.M.M., Appavoo, K., Sfeir, M.Y., Tretiak, S., Ajayan, P.M., Kanatzidis, M.G., Even, J., Crochet, J.J., Mohite, A.D., 2017. Extremely efficient internal exciton dissociation through edge states in layered 2D perovskites. Science 355, 1288–1292.

Brik, M.G., Kityk, I.V., 2011. Modeling of lattice constant and their relations with ionic radii and electronegativity of constituting ions of A_2XY_6 cubic crystals (A = K, Cs, Rb, Tl; X = tetravalent cation, Y = F, Cl, Br, I). J. Phys. Chem. Solids 72, 1256–1260.

Chen, Q., Zhou, H., Fang, Y., Stieg, A.Z., Song, T.-B., Wang, H.H., Xu, X., Liu, Y., Lu, S., You, J., Sun, P., McKay, J., Goorsky, M.S., Yang, Y., 2015. The optoelectronic role of chlorine in CH3NH3PbI3(Cl)-based perovskite solar cells. Nat. Commun. 6, 7269-1–7269-9.

Ciofini, I., Adamo, C., Chemette, H., 2005. Self-interaction error in density functional theory: a mean-field correction for molecules and large systems. Chem. Phys. 309, 67–79.

Deotale, A.J., Nandedkar, R.V., 2016. Correlation between particle size, strain and band gap of iron oxide nanoparticles. Mater. Today:. Proc. 3, 2069–20176.

Geisler, B., Blanca-Romero, A., Pentcheva, R., 2017. Design of n- and p-type oxide thermoelectrics in $LaNiO_3/SrTiO_3$(0 0 1) superlattices exploiting interface polarity. Phys. Rev. B. 95, 125301-1–11.

Hao, F., Stoumpos, C.C., Chang, R.P.H., Kanatzidis, M.G., 2014. Anomalous band gap behavior in mixed Sn and Pb perovskites enables broadening of absorption spectrum in solar cells. J. Am. Chem. 136, 8094–8099.

Hong, A.J., Yuan, C.L., Gu, G., Liu, J.-M., 2017. Novel p-type thermoelectric materials Cu_3MCh_4 (M = V, Nb, Ta; Ch = Se, Te): high band-degeneracy. J. Mater. Chem. A 5, 9785–9792.

Hu, X.K., Jood, P., Ohta, M., Kunii, M., Nagase, K., Nishiate, H., Kanatzidis, M.G., Yamamoto, A., 2016. Power generation from nanostructured PbTe-based thermoelectrics: comprehensive development from materials to modules. Energy Environ. Sci. 9, 517–529.

Kumar, P., Soni, A., Bhamu, K.C., Sahariya, J., 2017. Optoelectronic behavioral study of defect-chalcopyrite semiconductors XGa_2Te_4 (X = Zn, Cd). Mater. Res. Bull. 86, 131–138.

Lee, B., Stoumpos, C.C., Zhou, N., Hao, F., Malliakas, C.D., Yeh, C., Marks, T.J., Kanatzidis, M.G., Chang, R.P.H., 2014. Air stable molecular semiconducting iodosalts for solar cell applications: Cs_2SnI_6, as a hole conductor. J. Am. Chem. Soc. 136, 15379–15385.

Liu, W., Hu, J., Zhang, S., Deng, M., Han, C.-G., Liu, Y., 2017. New trends, strategies and opportunities in thermoelectric materials: a perspective. Mater. Today Phys. 1, 50–60.

Madsen, G.K.H., Singh, D.J., 2006. BoltzTraP. A code for calculating band-structure dependent quantities. Comput. Phys. Commun. 175, 67–71.

Maughan, A.E., Ganose, A.M., Bordelon, M.M., Miller, E.M., Scanlon, D.O., Neilson, J.R., 2016. Defect tolerance to intolerance in the vacancy-ordered double perovskite semiconductors Cs_2SnI_6 and Cs_2TeI_6. J. Am. Chem. Soc. 138, 8453–8464.

Murtaza, G., Ahmad, I., 2011. First principle study of the structural and optoelectronic properties of cubic perovskites $CsPbM_3$ (M = Cl, Br, I). Phys. B 406, 3222–3229.

Parker, D., Singh, D.J., 2011a. Potential thermoelectric performance from optimization of hole-doped Bi_2Se_3. Phys. Rev. X 1, 021005-1–021005-9.

Parker, D., Singh, D.J., 2011b. Transport properties of hole-doped CuBiS2. Phys. Rev. B 83, 233206-1–233206-4.

Penn, D.R., 1962. Wave-number-dependent dielectric function of semiconductors. Phys. Rev. 128, 2093–2097.

Perdew, J.P., Ruzsinszky, A., Csonka, G.I., Vydrov, O.A., Scuseria, G.E., Constantin, L.A.,

Zhou, X., Burke, K., 2008. Restoring the density-gradient expansion for exchange in solids and surfaces. Phys. Rev. Lett. 100 (13), 136406-1–136406-4.
Poudel, B., Hao, Q., Ma, Y., Lan, Y.C., Austin, M., Yu, B., Yan, X., Wang, D.Z., Muto, A., Vashaee, D., Chen, X.Y., Liu, J.M., Dresselhaus, M.S., Chen, G., Ren, Z.F., 2008. High-thermoelectric performance of nanostructured bismuth antimony telluride bulk alloys. Science 320, 634–638.
Protesescu, L., Yakunin, S., Bodnarchuk, M.I., Krieg, F., Caputo, R., Hendon, C.H., Yang, R.X., Walsh, A., Kovalenko, M.V., 2015. Nanocrystals of cesium lead halide perovskites ($CsPbX_3$, X = Cl, Br, and I): novel optoelectronic materials showing bright emission with wide color gamut. Nano Lett. 15, 3692–3696.
Qiu, X., Cao, B., Yuan, S., Chen, X., Qiu, Z., Jiang, Y., Ye, Q., Wang, H., Zeng, H., Liu, J., Kanatzidis, M.G., 2017. From unstable $CsSnI_3$ to air-stable Cs_2SnI_6: a lead-free perovskite solar cell light absorber with band gap of 1.48 eV and high absorption coefficient. Solar Energy Mater. & Solar Cells 159, 227–234.
Ran, C., Wu, Z., Xi, J., Yuan, F., Dong, H., Lei, T., He, X., Hou, X., 2017. Construction of compact methylammonium bismuth iodide film promoting lead-free inverted planar heterojunction organohalide solar cells with open-circuit voltage over 0.8 V. J. Phys. Chem. Lett. 8, 394–400.
Reshak, A.H., Khan, S.A., Auluck, S., 2014. Thermoelectric properties of a single graphene sheet and its derivatives. J. Mater. Chem. C 2, 2346–2352.
Reshak, A.H., Auluck, S., 2015. Thermoelectric properties of Nowotny-Juza NaZnX (X = P, As and Sb) compounds. Comput. Mater. Sci. 96, 90–95.
Rhyee, J.S., Cho, E., Ahn, K., Lee, K.H., Lee, S.M., 2010. Thermoelectric properties of bipolar diffusion effect on $In_4Se_{3-x}Te_x$ compounds. Appl. Phys. Letts. 97, 152104-1–3.
Saeed, Y., Singh, N., Schwingenschlögl, U., 2014. Thickness and strain effects on the thermoelectric transport in nanostructured Bi2Se_3. Appl. Phys. Lett. 105, 031915-1–031915-4.
Sakai, N., Haghighirad, A.A., Filip, M.R., Nayak, P.K., Nayak, S., Ramadan, A., Wang, Z., Giustino, F., Snaith, H.J., 2017. Solution-processed cesium hexabromopalladate(IV), Cs_2PdBr_6, for optoelectronic applications. J. Am. Chem. Soc. 139, 6030–6033.
Sharma, S., Schwingenschlögl, U., 2016. Thermoelectric response in single quintuple layer Bi_2Te_3. ACS Energy Lett. 1, 875–879.
Shuai, J., Mao, J., Song, S., Zhang, Q., Chen, G., Ren, Z., 2017. Recent progress and future challenges on thermoelectric Zintl materials. Mater. Today Phys. 1, 74–95.
Singh, D.J., 2010. Electronic structure calculations with the Tran-Blaha modified Becke-Johnson density functional. Phys. Rev. B 82, 205102-1–10.
Snyder, G.J., Toberer, E.S., 2008. Complex thermoelectric materials. Nat. Mater. 7, 105–114.
Sun, J., Shuai, J., Ren, Z., Singh, D.J., 2017. Computational modelling of the thermoelectric properties of p-type Zintl compound $CaMg_2Bi_2$. Mater. Today Phys. 1, 40–45.
Tran, F., Blaha, P., 2009. Accurate band gaps of semiconductors and insulators with a semilocal exchange-correlation potential. Phys. Rev. Lett. 102 (22), 226401-1–226401-4.
Wang, G., Wang, D., Shi, X., 2015. Electronic structure and optical properties of Cs2AX′2X4 (A = Ge, Sn, Pb; X′, X = Cl, Br, I). AIP Adv. 5, 127224-1–127224-7.
Xiao, Z., Zhou, Y., Hosono, H., Kamiya, T., 2015. Intrinsic defects in photovoltaic perovskite variant Cs_2SnI_6. PCCP 17, 18900–18903.
Zhang, J., Yu, C., Wang, L., Li, Y., Ren, Y., Shum, K., 2014. Energy barrier at the N719-dye/$CsSnI_3$ interface for photogenerated holes in dye-sensitized solar cells. Sci. Rep. 4, 6954-1–6954-6.
Zhang, D., Eaton, S.W., Yu, Y., Dou, L., Yang, P., 2015. Solution-phase synthesis of cesium lead halide perovskite nanowires. J. Am. Chem. Soc. 137, 9230–9233.
Zhang, Q.H., Liao, J.C., Tang, Y.S., Gu, M., Ming, C., Qiu, P.F., Bai, S.Q., Shi, X., Uher, C., Chen, L.D., 2017. Realizing thermoelectric conversion efficiency of 12% in Bismuth Telluride/Skutterudite segmented modules through full parameter optimization and energy-loss minimized integration. Energy Environ. Sci. 10, 956–963.
Zhao, L.-D., Lo, S.-H., Zhang, Y., Sun, H., Tan, G., Uher, C., Wolverton, C., Dravid, V.P., Kanatzidis, M.G., 2014. Ultralow thermal conductivity and high thermoelectric figure of merit in SnSe crystals. Nature 508, 373–377.